Near-field imaging in the megahertz range by strongly coupled magnetoinductive surfaces: Experiment and *ab initio* analysis

Cite as: J. Appl. Phys. **100**, 063105 (2006); https://doi.org/10.1063/1.2349469
Submitted: 28 February 2006 . Accepted: 14 July 2006 . Published Online: 25 September 2006

Manuel J. Freire, and Ricardo Marques

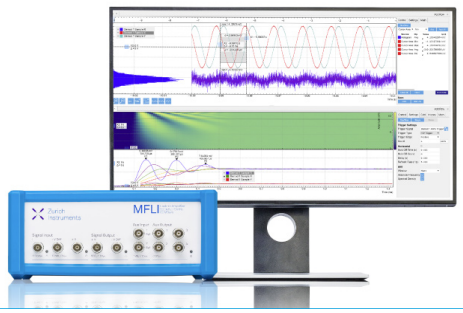

Near-field imaging in the megahertz range by strongly coupled magnetoinductive surfaces: Experiment and *ab initio* analysis

Manuel J. Freire[a] and Ricardo Marques
Departamento de Electrnica y Electromagnetismo, Facultad de Fisica, Universidad de Sevilla, Avenida Reina Mercedes s/n, E 41012 Sevilla, Spain

(Received 28 February 2006; accepted 14 July 2006; published online 25 September 2006)

In this work, the previously reported near-field imaging by two strongly coupled arrays of planar magnetic resonators is further studied. Experiments are performed to clarify the physical mechanisms underlying such an effect. The specific aim of these experiments is to clarify both the role played by magnetoinductive surface waves (MISWs) and the presence in the device of evanescent Fourier harmonics amplification. In addition to the experimental work, an *ab initio* theoretical analysis is developed to obtain a first approximation of the above effects. This model assumes that MISWs play the same role as plasmon-polaritons in negative refractive slabs, thus producing amplification of evanescent Fourier harmonics in the device. It also predicts that imaging occurs close to the resonators' resonant frequency, between the passbands for the two MISW branches that can be excited in the lens. Both predictions from the theoretical model are in qualitative agreement with the experimental results. Quantitative agreement can also be obtained if some appropriate additional hypotheses, taking into account the discrete nature of the present device, are included in the model. The reported results suggest the possibility of using this kind of device for imaging in the megahertz range such as in nuclear magnetic resonance imaging. © *2006 American Institute of Physics*. [DOI: 10.1063/1.2349469]

I. INTRODUCTION

After the seminal works of Veselago[1] and Pendry,[2] imaging by metamaterial slabs became an active area of research. Although losses may substantially degrade this effect,[3] they do not prevent the onset of subdiffraction images in near-field experiments.[4–6] In fact, near-field subdiffraction imaging by metamaterial slabs[2] has been reported in experiments carried out with a two-dimensional circuit analogous to a left-handed medium,[7] a single-cell-depth left-handed slab,[8] a silver slab operating at optical frequencies,[9] a pair of magnetoinductive surfaces,[10] and a photonic crystal flat lens.[11] In addition, it has been predicted for ferrite slabs[12] and in a pair of coupled resonant impedance surfaces[13] (in this last work, amplification of evanescent modes was also experimentally shown). The main aim of this paper is to develop further the analysis of the magnetoinductive (MI) lens previously reported by the authors in Ref. 10. In particular, the role of magnetoinductive surface wave[14] (MISW) for image formation will be clarified, and the field distribution at the image plane will be studied.

The MI lens analyzed[10] is a near-field imaging device consisting of two parallel planar periodic arrays of inductively coupled resonators[10] that can be designed to work at frequencies ranging from megahertz to terahertz. In the present work, the resonators are capacitively loaded open metallic rings (CLORs). In the resulting device, the imaging is closely related to the excitation of MISW (Ref. 14) at each individual array of resonators.[10] However, we have found that imaging does not occur at those frequencies where MISWs are excited in the device. In fact, when two CLOR arrays are coupled in order to form the MI lens, the single-array MISW dispersion relation splits into two branches, with passbands above and below the passband of the original MISW's isolated array dispersion relation. We have found that the excitation of either of these MISW branches is undesirable for image formation, because it would imply resonances due to the excitation of surface waves in the plane of the device, and image distortion by the disproportionate contribution of such resonances. A similar conclusion was previously reported regarding plasmon-polariton excitation in imaging devices made of negative permittivity slabs.[15] In order to avoid this undesirable effect, the coupling between both arrays of resonators must be strong enough to produce a clear separation between the passbands of both MISW branches. When this condition is achieved, we have observed image formation at some frequencies between the passbands for both MISW branches. For this reason, strongly coupled CLOR arrays are considered in this work. In the reported experiments, the source was initially located at a distance from the lens equal to the distance between the CLOR arrays. We have found that in this configuration, the image is formed just at the exit of the lens. The above configuration is expected to reduce losses in the CLOR arrays and will thus be optimal with regard to resolution.[16] Moreover, this configuration has previously been used in other subdiffraction image experiments carried out in the optical range of frequencies.[9] In subsequent experiments in this paper, the effect of varying the distance between the source and the lens was studied and a significant enhancement of the image field was observed when the source approaches the lens.

With regard to field measurements at the image plane, care must be taken in order to avoid artifacts coming from

[a]Electronic mail: freire@us.es

the matching capabilities of the lens.[17,18] As was previously clarified in such papers, the information for subdiffraction image formation is carried by the source field evanescent Fourier harmonics (FHs). Although it is well known that evanescent electromagnetic waves do not carry power, any field measurement implies some flux of energy between the source and the detector and thus a substantial perturbation of the evanescent field. Therefore, if inappropriate detectors are used, the measurement procedure will substantially affect the field at the image, and the behavior of the lens may be closer to a tunneling device than to an imaging device.[18] Although for some applications such a tunneling effect may be of interest, it must be avoided for the particular purpose of this work. In order to avoid this effect, very small detectors with a sufficiently low input impedance have been used during the measurements. This choice ensures that the detected field does indeed correspond to a direct measurement of the field created behind the lens by the source alone.[18]

In order to develop an *ab initio* analysis of the studied phenomena, a theoretical quasianalytical model is also proposed in this work. This analysis assumes a surface impedance model for each array of resonators. The transfer function of the lens is obtained following the method previously proposed in Ref. 13. The above MISW branches appear as poles of this transfer function. Between such poles, a flat transfer function with an almost constant value near unity at the image plane is found, thus justifying the image formation. Although such a model is a continuous model neglecting the discrete nature of the device, it has been found to be in good qualitative agreement with the experimental results. In particular, it predicts the observed image formation at some frequencies between the two MISW branches of the device. It also predicts the observed image formation when the distance between the source and the image is twice the distance between the resonator arrays. Finally, it also predicts the observed enhancement of the image field when the source approaches the lens. When some additional hypotheses that take into account the discrete nature of the MI lens and that of the detector are included in the model, a good quantitative agreement between the model and the experiments can also be obtained.

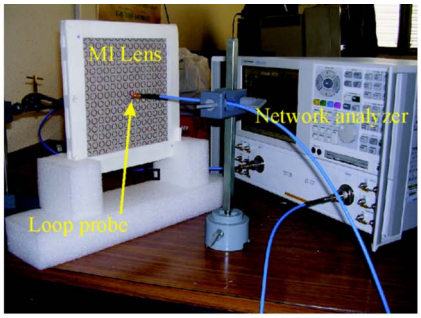

(a)

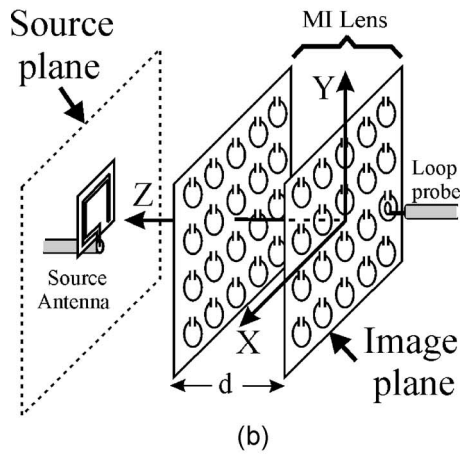

(b)

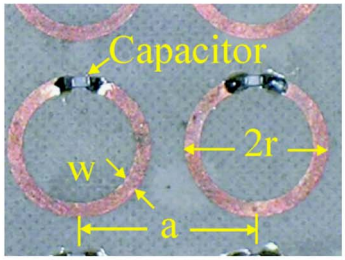

(c)

FIG. 1. (Color online) (a) Photograph of the experimental setup. (b) Schematic view of the experimental procedure. (c) Detail of the capacitively loaded rings forming the MI lens.

II. EXPERIMENT

A MI lens operating in the radio-frequency range was fabricated. The lens consisted of two plane arrays of CLOR, placed parallel and separated by a distance $d=4.5$ mm. The periodicity of the arrays is $a=12.5$ mm. Each array has 14×14 resonators fabricated by photoetching planar open metallic loops on a low-permittivity dielectric substrate. Surface-mounted capacitors (nominally $C=82$ pF) were soldered into the gap of each loop. The external diameter of each loop is 1 cm and the width of the metallic strip in the loop is 1 mm. The experimental setup, including a detail of the ring resonators, is shown in Fig. 1. The resonance frequencies of the rings on the array were measured, and it was found that all of them fall inside the range $\omega_0/(2\pi)=137.5$ MHz$\pm2\%$. The ring's self-inductance was calculated from this value and from the value of the above capacitance $C=82$ pF. This calculation provided the value $L=16.3$ nH. The source, shown in Fig. 2, was a square-shaped narrow parallel-strip transmission line, short circuited at the end. The total length of the transmission line is approximately $8a=10$ cm, much smaller than the wavelength at 140 MHz, $\lambda\simeq200$ cm. Therefore, the current can be considered as being almost uniform along the transmission line. The parallel-wire line was sharp bended in order to produce a strong and uniform square-shaped magnetic field crest in the source plane. Each side length of this square-shaped crest is $2a$ (a is the distance between two consecutive rings in the MI lens). The probe used for field measurements was the small loop antenna shown in Fig. 2. The loop radius was 4 mm, and its measured input reactance was 10.7 Ω, well below the value of the characteristic impedance of the input and output coaxial waveguides $Z_0=50$ Ω. This loop reactance value ensures that the transmission coefficient between the source

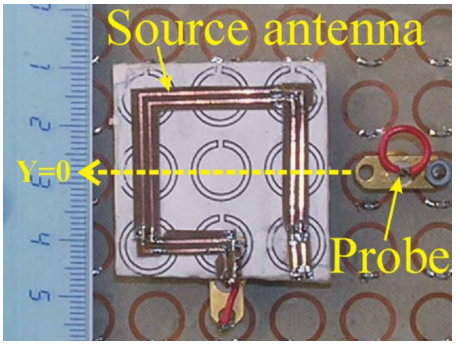

FIG. 2. (Color online) Photograph of the antennae used as source and probe. A paper sheet with the ring contours drawn on it was placed below the source antenna in order to illustrate their relative locations during the experiments. The dotted line shows the line along which the measurements of Fig. 5 were made.

and the probe does indeed correspond to a measurement of the field as it exists in the absence of the detector.[18] In the experiments, the source is placed in front of the lens (at different distances from it), so that the magnetic crest passes through the centers of eight consecutive rings, leaving a single ring at its center (see Fig. 2). The image plane is fixed at the exit interface of the lens (as already mentioned, this configuration improves resolution[16]). For the measurements, the probe is placed at the center of each ring at the exit interface of the lens successively. The measured transmission coefficient between the source and the probe provides a map of the field at the image plane. An Agilent Technologies network analyzer E8363B was used to measure the transmission coefficient between the source and the probe.

Before proceeding to measure the images directly, the frequency at which such images are formed must be determined. For this purpose, the source was placed at the input interface of the lens [$z=d$ in Fig. 1(b)] and the probe was placed at the exit interface of the lens [$z=0$ in Fig. 1(b)] and at the center of the ring, placed precisely in the center of the source. A plot of the transmission coefficient measured at different frequencies is shown in Fig. 3. We interpret the two peaks centered at 130 and 150 MHz to correspond to the excitation of the two MISW branches of the device (see next section for a detailed explanation). The middle point in the curve of Fig. 3 corresponds to a frequency of approximately 140 MHz. We choose this frequency, where the effect of the MISW branches is minimized, as the proper frequency for image measurements. Once the frequency for the image formation was determined, the image formed at the exit interface of the lens, with the source placed at different distances, was measured. The results of such measurements at the frequency of 140 MHz, obtained following the above method, are shown in Fig. 4. Figure 4(a) shows a map of the field intensity measured at the source plane without the lens. Figure 4(b) shows a map of the field intensity at the exit interface of the lens, when the source is placed at a distance of $2d$ from the interface. Finally, Fig. 4(c) shows a map of the field at the exit interface of the lens, when the source is placed at a distance of $1.5d$ from the interface. The scale in all figures is the same, and for data collection the probe was moved in identical steps (length a) along the coordinate axes in the

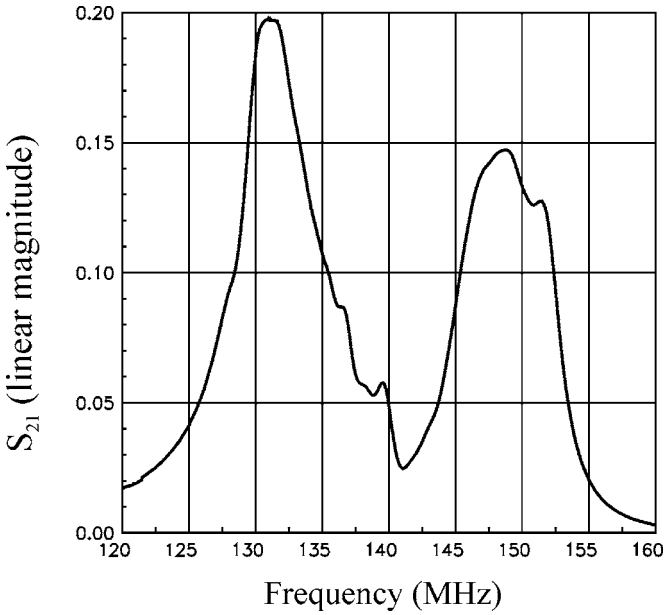

FIG. 3. Plot of the transmission coefficient between the source and the probe, when the probe is located over the central ring of the lens, and the source at a distance d from the exit interface of the lens.

measurement plane. The formation of a clear image of the source can be observed in Fig. 4(b), where it can also be observed that the field intensity at the source is reproduced quite well at the image. The image seen in Fig. 4(c) seems to reproduce approximately the form of the source, but with a substantial enhancement of the field intensity at the cost of some distortion. We feel that the reported results clearly show that the image is formed at a distance $2d$ from the source (d being the width of the lens), and there is a significant enhancement of the field when the source approaches the lens, which is in agreement with FH amplification inside the device.

In order to obtain a better picture of the lens resolution, the measurement of the field intensity along the line marked in Fig. 2 is plotted in Fig. 5 for different source distances. For comparison purposes, two plots of the measurement of the field intensity along this line at the source plane and at a distance $2d$ from the source in air (without the lens) are also included in the figure. The curve corresponding to the field intensity measured at the exit interface of the lens with the source placed at a distance $2d$ from this interface approximates the curve showing the field intensity at the source plane reasonably well. This fact corroborates our previous theoretical predictions about image formation in the MI lens.[10] The curves corresponding to smaller distances between the source and the image clearly show an enhancement of the field intensity at the lens' exit interface something that is also in agreement with our previous theoretical analysis.[10,18] Finally, the overall effect of the lens on the image formation can be appreciated by comparing the field in the presence of the lens with the curve showing the field intensity in air, at a distance $2d$ from the source (i.e., in the absence of the lens).

It is of interest to investigate the behavior of the lens at those frequencies where the MISW shown in Fig. 3 can be

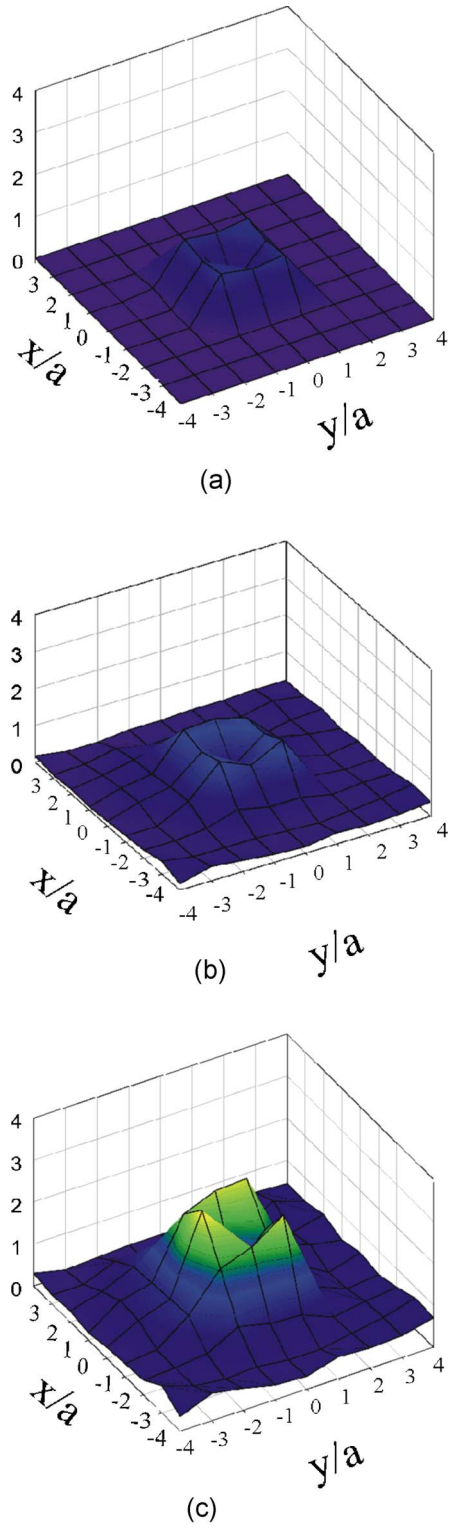

FIG. 4. (Color online) (a) Map of the z component of the magnetic field intensity at the source plane. (b) Map of the z component of the magnetic field intensity at the image plane (exit of the lens), when the source is located at a distance $2d$ from the image plane. (c) Map of the z component of the magnetic field intensity at the image plane (exit of the lens), when the source is located at a distance $1.5d$ from the image plane.

excited. The "image" formed when the source is placed at a distance $2d$ from the image plane (the exit interface of the lens) is shown in Fig. 6 for a frequency of 130 MHz. It can be clearly observed that, in spite of the high transmission level at the central ring, the image is not formed at all. This

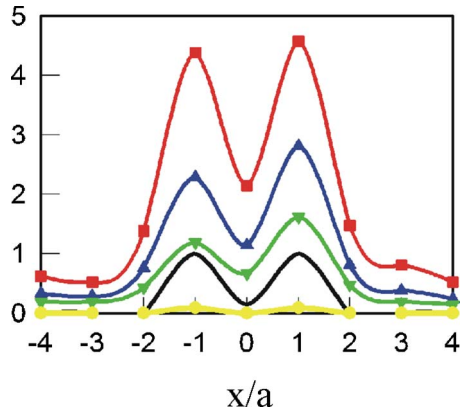

FIG. 5. (Color online) Field profiles along the dotted line of Fig. 2 for different distances between the source and the image plane (at the exit of the lens): d (■), $1.5d$ (▲), and $2d$ (▼). The field at the source plane (black solid line) as well as the field measured in air (●), without the lens, at a distance $2d$ from the source plane are also shown.

result clearly shows the importance of avoiding the excitation of MISW if good images are desired. For this purpose, both CLOR arrays must be strongly coupled, so that the frequency passbands of both MISWs do not overlap. This fact seems to be the main limitation for manufacturing MI lenses of a greater thickness that would enable images to be formed further from the source. For this purpose, a reduction of the bandwidth of the MISW supported by the lens would be desirable. Since this bandwidth is mainly given by the M/L ratio,[14] a good strategy may be to design magnetic resonators with higher self-inductances while keeping the mutual inductance constant. The use of Swiss rolls[19] instead of capacitively loaded open rings seems to be a promising alternative in this direction. Future works will explore this and other possibilities.

In summary, the reported experiments strongly suggest that the mechanism for image formation in MI lenses is qualitatively similar to image formation mechanisms in other previously reported metamaterial superlenses,[2–13] the image being formed due to the amplification of evanescent FHs inside the lens, and to a restoration of this amplitude at a distance $2d$ from the source. The reported experiments also

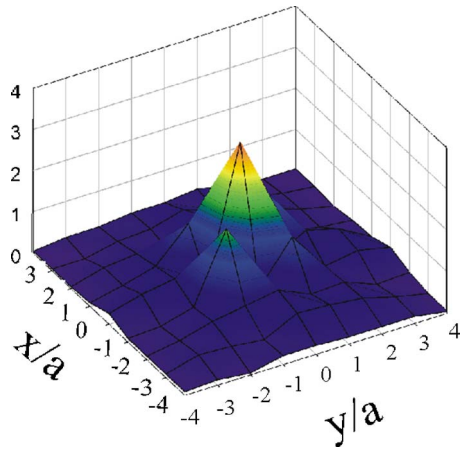

FIG. 6. (Color online) Image formed at the exit interface of the lens, under the same circumstances as in Fig. 4(b) but at the frequency $\omega/(2\pi) = 130$ MHz, corresponding the left peak of Fig. 3.

suggest that MISW in MI lenses play the same role as other surface waves (surface plasmon-polaritons or surface magnetostatic waves) in the above devices.[2–13] Finally, it has been firmly established that image formation takes place at frequencies lying between the two MISW branches of the device.

III. THEORETICAL MODEL

In order to gain physical insight on the reported experimental results, an *ab initio* theoretical model has been developed. In this model we will neglect, as a first approximation, the discrete nature of the CLOR arrays and will assume a surface impedance model for them. The transfer function for the resulting system of closely coupled impedance surfaces will be obtained following the procedure previously reported in Ref. 13, after some modifications introduced in order to take into account the magnetic nature of the CLOR resonators. Although the main steps for this analysis are actually described in Ref. 13, they will be briefly outlined here for completeness. Using the same notation as in the above paper, the complex amplitudes of waves traveling (or decaying) in opposite directions across the device are related by a 2×2 transmission matrix as

$$\begin{bmatrix} E_2^- \\ E_2^+ \end{bmatrix} = T_{\text{tot}} \begin{bmatrix} E_1^- \\ E_1^+ \end{bmatrix}, \quad T_{\text{tot}} = \begin{bmatrix} t_{11} & t_{12} \\ t_{21} & t_{22} \end{bmatrix}, \tag{1}$$

where $E_1^{\pm}$ and $E_1^{\pm}$ denote the tangential components of the electric field complex amplitude at both the source and the image plane (subscript 1 denotes the source plane and subscript 2 denotes the image plane). The signs $\pm$ correspond to the signs in the exponential term $\exp(\pm ikz)$ of these waves, z being the axis perpendicular to the lens, and k the propagation constant along this direction. The transfer function T can be obtained form the above transmission matrix T_{tot} as

$$T = \left.\frac{E_2^-}{E_1^-}\right|_{E_2^+=0} = t_{11} - \frac{t_{12}t_{21}}{t_{22}}. \tag{2}$$

In the experiments reported in this work, the image plane is fixed at the exit of the lens, and the source plane is placed at a certain distance from the lens due to the fact that, as has already been mentioned, this configuration is optimal with regard to resolution.[16] Taking this into account, the transmission matrix T_{tot} can be written as

$$T_{\text{tot}} = T_{\text{lens}} T_{\text{sp before}}, \tag{3}$$

where T_{lens} is the transmission matrix of the lens and $T_{\text{sp before}}$ represents the transmission matrix for the air layer occupying the space between the source plane and the lens. Denoting by d the thickness of the lens, if the source plane is placed at the same distance d from the lens, $T_{\text{sp before}}$ is as follows:

$$T_{\text{sp before}} = \begin{bmatrix} \exp(-jkd) & 0 \\ 0 & \exp(+jkd) \end{bmatrix}, \tag{4}$$

where $k=\sqrt{k_0^2-k_x^2-k_y^2}$. Moreover, T_{lens} can be written as

$$T_{\text{lens}} = T_{\text{out}} T_{\text{sp(d)}} T_{\text{in}}, \tag{5}$$

where T_{in} and T_{out} are the matrices describing the two arrays of resonators. In our case both matrices are identical and can be written as[13]

$$T_{\text{in}} = T_{\text{out}} = \begin{bmatrix} 1-\eta_0/2Z_g & -\eta_0/2Z_g \\ \eta_0/2Z_g & 1+\eta_0/2Z_g \end{bmatrix}, \tag{6}$$

where Z_g is the surface impedance of the array of resonators and η_0 is the wave impedance of a vacuum. The grid impedance Z_g is expressed as function of the so-called cell impedance Z_c as[13]

$$Z_g = Z_c - \frac{\eta_0}{2}, \tag{7}$$

where Z_c is the impedance relating the average surface current density $\mathbf{J}$ on the array and the external electric field $\mathbf{E}_{\text{ext}}$ imposed by the source, that is,

$$\mathbf{E}_{\text{ext}} = Z_c \mathbf{J}. \tag{8}$$

In the MI lens, the resonators are excited by the z component of the external magnetic field $\mathbf{H}_{\text{ext}}$ imposed by the source. For our analysis, it is then convenient to obtain the relation between $H_{\text{ext},z}$ and $\mathbf{E}_{\text{ext}}$. This relation directly follows from $\nabla\times\mathbf{E}=i\omega\mu_0\mathbf{H}$, i.e.,

$$H_{\text{ext},z} = \frac{\mathbf{k}_t \times \mathbf{E}_{\text{ext}}}{\omega\mu_0} \cdot \hat{\mathbf{z}}, \tag{9}$$

where $\mathbf{k}_t=k_x\hat{\mathbf{x}}+k_y\hat{\mathbf{y}}$ is the wave vector along the array. Next, on the array, the averaged surface current density $\mathbf{J}$ can be obtained from the averaged magnetic moment $\mathbf{M}$ through $\nabla\times\mathbf{M}=\mathbf{J}$. Therefore

$$\mathbf{J} = -\frac{1}{a^2}(i\mathbf{k}_t \times \mathbf{m}), \tag{10}$$

where a is the array's periodicity and $\mathbf{m}$ is the magnetic moment for each resonator. Taking into account (8)–(10), Z_c can be expressed as

$$Z_c = -\frac{i\omega\mu_0 a^2 H_{\text{ext}}}{m(k_x^2+k_y^2)}. \tag{11}$$

The magnetic moment and the external magnetic field are then related through

$$m = \chi(\omega)[H_{\text{ext}} + \beta(\omega,k_t)m], \tag{12}$$

where $\chi(\omega)$ is the resonator polarizability and $\beta(\omega,k_t)$ an interaction factor, which takes into account the inter-resonator coupling. Thus, taking into account (11) and (12), Z_c can be written as

$$Z_c = -\frac{i\omega\mu_0 a^2}{(k_x^2+k_y^2)}\left[\frac{1}{\chi(\omega)} - \beta(\omega,k_t)\right]. \tag{13}$$

Next, it is shown that both $\chi(\omega)$ and $\beta(\omega,k_t)$ can be derived from the dispersion relation of the MI waves propagating in a single two-dimensional (2D) array of resonators under the influence of the external magnetic field. This dispersion relation can be obtained from the circuit equation for a single resonator,[14]

$$\left(R + i\omega L + \frac{1}{i\omega C}\right) I = i\omega M 2I[\cos(k_x a) + \cos(k_y a)] + i\omega\mu_0 H_{\text{ext}} S_0, \tag{14}$$

where I is the intensity of the ring, R, L, and C are the resistance, self-inductance, and capacitance of each resonator, respectively, and M is the mutual inductance between the nearest resonators in the array. The first term on the right side of (14) accounts for the voltage induced on each resonator by its four nearest neighbors,[14] whereas the second term accounts for the voltage induced by the external magnetic field. Taking into account that $m=IS_0$, where S_0 is the effective ring surface, the magnetic moment can be obtained as follows:

$$m = \frac{\mu_0 S_0^2 \omega^2}{L(\omega_0^2 - \omega^2) + i\omega R} \times \left\{ H_{\text{ext}} + m\frac{2M}{\mu_0 S_0^2}[\cos(k_x a) + \cos(k_y a)] \right\}. \tag{15}$$

Comparing both (12) and (15), the following expressions for $\chi(\omega)$ and $\beta(\omega, k_t)$ are obtained:

$$\chi(\omega) = \frac{\mu_0 S_0^2 \omega^2}{L(\omega_0^2 - \omega^2) + i\omega R}, \tag{16}$$

$$\beta(\omega, k_t) = \frac{2M}{\mu_0 S_0^2}[\cos(k_x a) + \cos(k_y a)].$$

Taking into account the fact that the resonators are excited by TE waves, with no electric field component along the z axis, the wave impedance η_0 must be taken as

$$\eta_0 = \frac{\omega\mu_0}{k}. \tag{17}$$

Thus, after substituting (16) and (17) in (13) and (7), the transmission coefficient or transfer function as given in (2) is calculated.

IV. COMPARISON BETWEEN THEORETICAL MODEL AND EXPERIMENT

Figure 7(a) shows a three-dimensional plot of the transfer function $T(\omega, k_x, k_y=0)$ when the source is placed at a distance $z=2d$ from the exit of the lens. The parameters, used for the calculation and given in the caption, are the same as in the experiments reported in Sec. III. The ring inductance was obtained from the CLOR's experimental resonance frequency ω_0 through $\omega_0^{-2}=LC$, and the mutual inductance was estimated by assuming that each ring is *seen* by its closest neighbors as a point dipole. We interpret that the peaks in the plot correspond to both MISW branches supported by the device, which appear as resonances of the transfer function. The periodicity of such MISW branches along the first and the second Brillouin zones can be clearly appreciated in the figure. A flat region of $T \simeq 1$ can be seen clearly between these peaks. From these results it is apparent that, for imaging applications, the operating frequency of the lens must be chosen between the passbands of both MISWs, close to the resonant frequency of the rings, $\omega_0/(2\pi)=137.5$ MHz. The transfer function $T(\omega_0, k_x, k_y=0)$ at the chosen frequency of operation $\omega/(2\pi)=140$ MHz is shown in Fig. 7(b). It can be clearly seen that this transfer function is very close to unity for almost all values of the wave number k_x. The transfer function has been plotted for values of k_x ranging in the interval $[0, \pi/r]$, where r is the averaged radius of the resonators in the experiment. The reason for this choice will be explained below.[21] It is worth mentioning that, if the distance between the arrays supporting the MISW increases, both MISW branches get closer, and where the transfer function is flat, the frequency region narrows. If the arrays are sufficiently far away, the MISW bands overlap around the resonant frequency of the rings and the imaging capabilities of the lens disappear. This is, according to the model, the main effect limiting the MI lens thickness and, therefore, the distance over which a source can be imaged. The plot of the transfer function shown in Fig. 7(a) predicts that the image is well formed only at frequencies around the resonant frequency. This prediction is in agreement with the measurements shown in Figs. 4(b) and 6, which show a correct formation of the image at 140 MHz and a bad formation of the

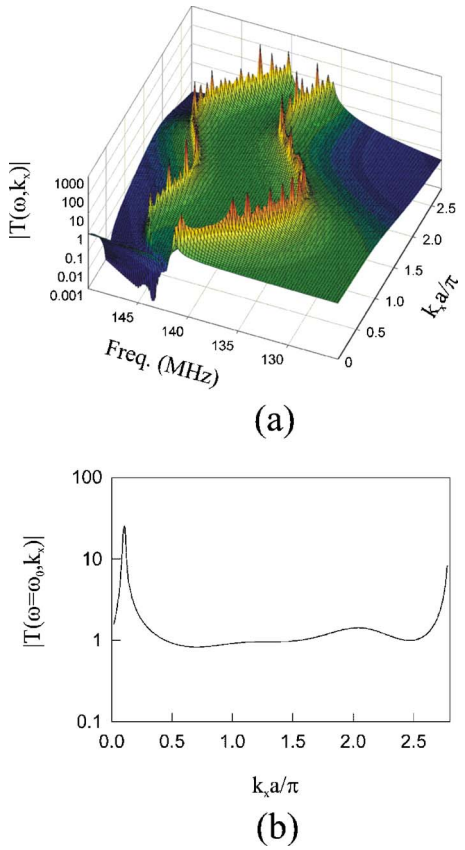

FIG. 7. (Color online) (a) Three-dimensional plot of the transfer function $T(\omega, k_x, k_y=0)$ for the lens of the experiment with the source placed at a distance $2d$ (d is the lens thickness) from the image plane, at the exit of the lens. The transfer function is calculated for the following parameters: $a=12.5$ mm, $R=0.04\ \Omega$, $C=82$ pF, $L=16.3$ nH, $\omega_0/(2\pi)=137.5$ MHz, and $M=-0.015L$ (the mutual inductance is negative because the magnetic field originating in a ring must change direction in order to cross another ring). The external radius of the resonator is 5 mm and the width of the ring is 1 mm, so that the resonator's effective area is $S_0=\pi r^2$, where an averaged radius $r=4.5$ mm is considered. (b) Two-dimensional plot of the transfer function $T(\omega, k_x, k_y=0)$ at $\omega/(2\pi)=140$ MHz.

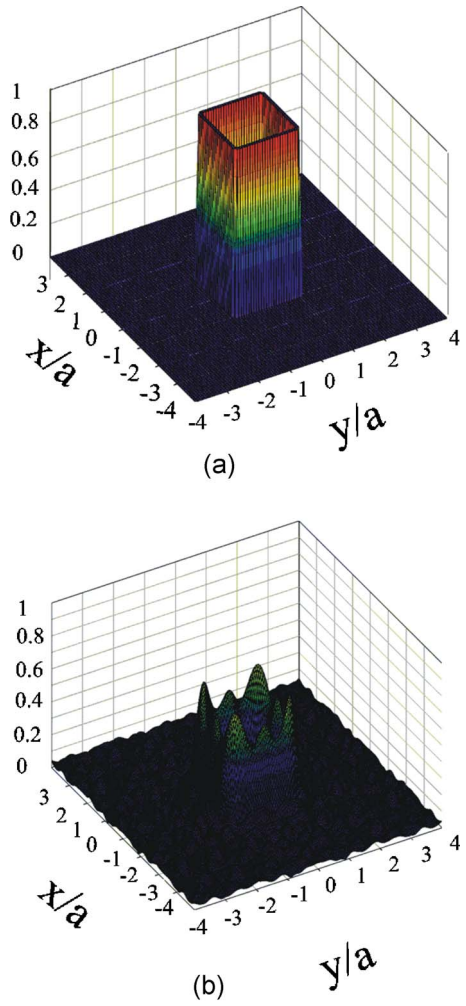

FIG. 8. (Color online) (a) Simulation of the z component of the magnetic field intensity in the plane of the source antenna shown in Fig. 2. (b) Map of the z component of the magnetic field intensity calculated at the image plane (exit of the lens), when the field source in (a) is imposed at a distance $2d$ from the image plane.

image at 130 MHz, respectively. Therefore, from a qualitative point of view, the theoretical model is in agreement with the experiment. Moreover, since the model provides the transfer function, it is possible to calculate from this function the field distribution at the image plane when the source is placed at any distance from it. The comparison between these calculations and the experimental results will provide a measurement of the quantitative agreement between the model and the experiment. In order to calculate the field distribution, a FORTRAN 90 code has been developed. The magnetic field along the z direction in the plane of the source antenna shown in Fig. 2 has been modeled by means of the square-shaped distribution shown in Fig. 8(a). The thickness of the wall in the field distribution is equal to the averaged distance between the parallel strips in the source antenna shown in Fig. 2, that is, 2 mm. The unit cell of the spatial grid used in the plot shown in Fig. 8(a) is $\Delta=0.5$ mm. The FHs of this field distribution are obtained for the different values of the spectral wave numbers k_x and k_y by means of a two-dimensional fast Fourier transform (FFT) algorithm[20] implemented in the FORTRAN 90 code. In the FFT algorithm, the Nyquist critical frequency[20] defines the interval of discretized values that the wave numbers k_x and k_y can take as $[-\pi/\Delta, \pi/\Delta]$. Since $\Delta=0.5$ mm and the period $a=12.5$ mm, it is of interest for the following discussion to note that this interval can be written as $[-25\pi/a, 25\pi/a]$. The FHs are multiplied by the corresponding value of the transfer function and then a FFT algorithm is used to obtain the inverse Fourier transform that provides the field distribution at the image plane. At this point, we have introduced an additional hypothesis into the analysis: only those FHs able to create a significant magnetic flux through the CLOR can excite them and, consequently, only such FHs can be reproduced by the lens. We feel that a good criterion for such choice is to take $|k_x|, |k_y| < \pi/r$, where r is the mean radius of the CLOR. FHs with $|k_x|, |k_y| > \pi/r$ will strongly oscillate along the CLOR diameter and will not excite them appreciably. Therefore, only the FHs corresponding to values of k_x and k_y in the interval $[-\pi/r, \pi/r]$ were used in the inverse Fourier transform to build the image. This hypothesis was validated by the quantitative agreement existing between the experimental results and the theoretical results. Figure 8(b) shows the calculated field distribution at the exit of the lens at a frequency of 140 MHz when the source field shown in Fig. 8(a) is imposed at a distance $z=2d$ from the image plane. The calculated field cannot be directly compared with the experimental results, since the measurements do not correspond to the image field but to the flux of the image field through the loop probe. Therefore, once the field distribution is calculated, it is integrated inside a circle with a radius equal to the radius of the loop probe. To build a plot which can be compared with the measurements, the centers of the integration area are chosen at the actual locations of the probe in the experiments. Figure 9(a) shows the magnetic flux of the source field shown in Fig. 8(a), calculated as described above and normalized to unity. Figure 9(b) shows the magnetic flux at the image plane of the field shown in Fig. 8(b) and normalized to the flux at the source plane when this source is placed at a distance $z=2d$. Finally, Fig. 9(c) shows the magnetic flux calculated at the image plane when the source is placed at a distance $z=1.5d$. The theoretical results shown in Figs. 9(a)–9(c) can be directly compared with the experimental results shown in Figs. 4(a)–4(c). The comparison shows a good quantitative agreement between both types of results. Figure 10 shows theoretical results for the image at a frequency of 130 MHz with the source at a distance $z=2d$ that are similar to the experimental results shown in Fig. 6 and which correspond to the distorted image due to the excitation of the MISW associated with the left peak in Fig. 3. Both theoretical and experimental results are in agreement in the sense that the image is not well formed at this frequency. Next, Fig. 11(a) shows calculated results similar to the experimental results shown in Fig. 5 for the field profile existing at the image for different source distances: $z=2d$, $z=1.5d$, and $z=d$. There is a good qualitative agreement with the experimental results shown in Fig. 5 and a good quantitative agreement at least for the cases corresponding to $z=2d$ and $z=1.5d$.

It may be of interest to investigate the effect of a different choice of the FH truncation in the FFT algorithm upon

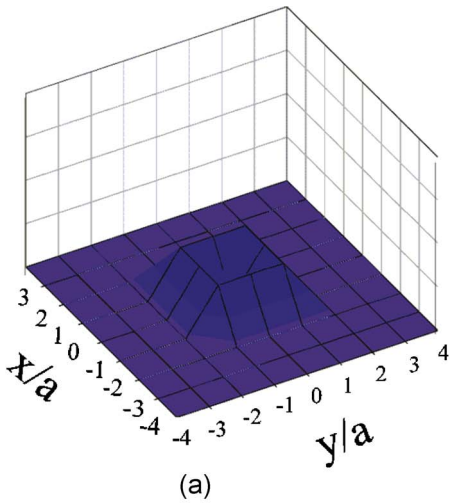

(a)

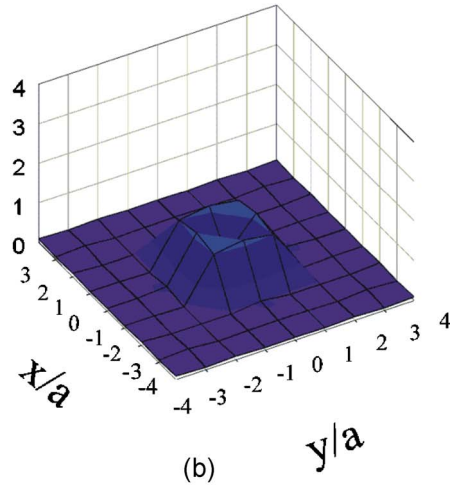

(b)

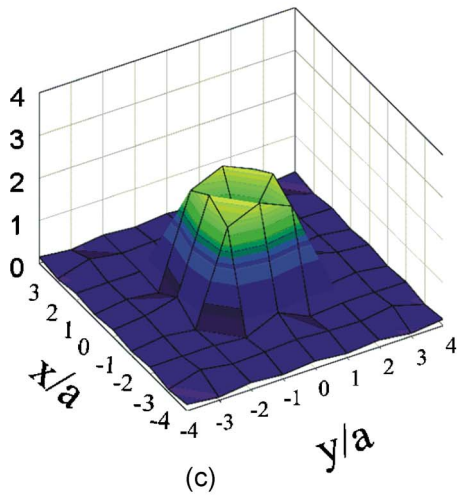

(c)

FIG. 9. (Color online) (a) Map of the flux of the z component of the magnetic field intensity imposed in the source plane and shown in Fig. 8(a). (b) Map of the flux of the z component of the magnetic field intensity calculated at the image plane (exit of the lens), when the source is located at a distance $2d$ from the image plane. (c) Map of the flux of the z component of the magnetic field intensity calculated at the image plane (exit of the lens), when the source is located at a distance $1.5d$ from the image plane. The flux is calculated as described in the text.

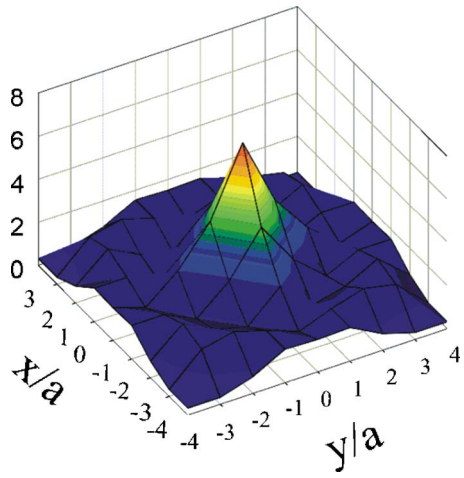

FIG. 10. (Color online) Computed image at the exit interface of the lens, under the same circumstances as in Fig. 9(b) but at the frequency $\omega/(2\pi)$ $=130$ MHz, corresponding to the left peak of Fig. 3.

the results provided by the model. Figure 11(b) shows the results obtained by building the image with the FHs corresponding to values of k_x and k_y in the interval $[-\pi/a, \pi/a]$. Figure 11(c) shows the results obtained by building the image with all the FHs generated by the FFT algorithm, that is, with the FHs corresponding to values of k_x and k_y in the interval $[-25\pi/a, 25\pi/a]$. The results in Figs. 11(b) and 11(c) are in qualitative agreement with the experimental results shown in Fig. 5. This qualitative agreement shows that the proposed model provides qualitative agreement with the experiments regardless of the particular hypothesis made about the truncation of the FH expansion. In addition, the quantitative agreement between Figs. 11(a) and 5 shows that, when the appropriate hypotheses on the FHs truncation are made, the model can also provide a reasonable quantitative agreement with the experiments.

V. CONCLUSION

Image formation in magnetoinductive lenses has been analyzed by experiments performed in the megahertz range. A lens composed of two strongly coupled magnetic resonator plane arrays has been built up. Experiments undertaken with this device have shown that image formation takes place at frequencies close to the resonance frequency of each individual resonator, between the two magnetoinductive surface wave branches of the coupled arrays. The best resolution was found when the distance from the source to the image was twice the lens width, and a substantial field enhancement was measured when the source approached the detector. All of these results strongly suggest that the image is formed through Fourier harmonics enhancement inside the device, according to the same schema of other previously reported metamaterial lenses. A theoretical model has been developed which predicts the main features of image formation in the studied device. This model makes the analogy existing between surface plasmons in negative refractive slabs and magnetoinductive surface waves in magnetoinductive lenses clear. A key conclusion of the model is that, for a correct image formation, the magnetoinductive lens should be thin

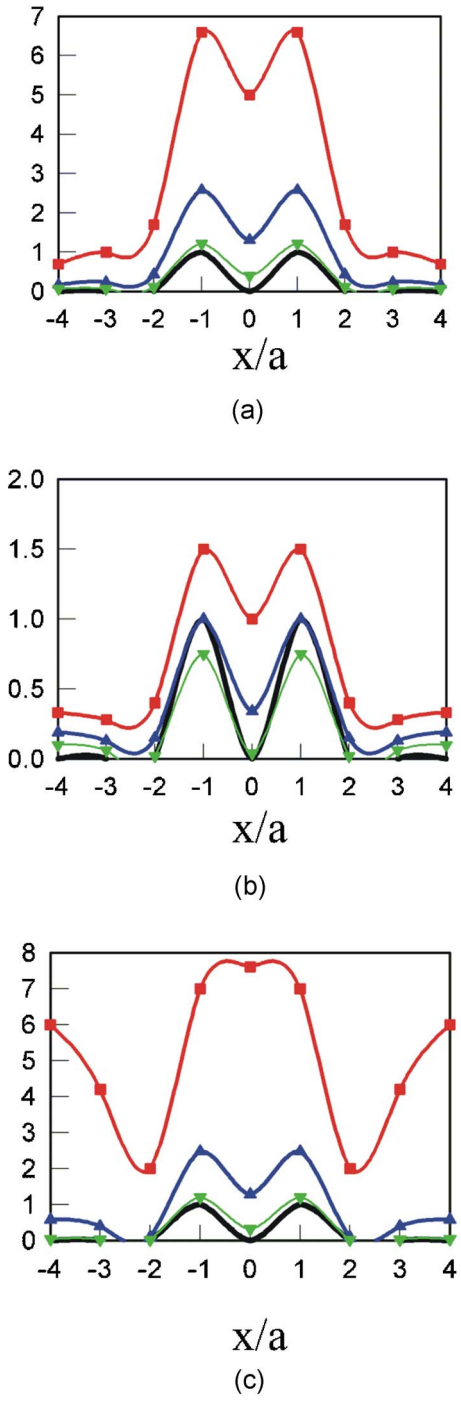

FIG. 11. (Color online) Calculation of flux profiles along the dotted line of Fig. 5 for different distances between the source and the image plane (at the exit of the lens) and by using the same method as is Fig. 9: d (■), $1.5d$ (▲), and $2d$ (▼). The flux at the source plane (solid black line) is also shown. The results are computed by truncating the FHs in the FFT algorithm to the intervals (a) $|k_x|, |k_y| < \pi/r$, (b) $|k_x|, |k_y| < \pi/a$, and (c) $|k_x|, |k_y| < 25\pi/a$ (i.e., all the FHs generated by the FFT algorithm).

enough to avoid the overlapping of the two magnetoinductive surface wave branches supported by the lens, and this seems to be the main practical limitation of such lenses. In our opinion, the reported experimental and theoretical results open the door for the design of practical subdiffraction imaging devices in the megahertz range, which may be of interests for nuclear magnetic resonance imaging and other applications.

ACKNOWLEDGMENTS

This work has been supported by Spanish Ministry of Education and Science (MEC) Directorate General for Research (DGI), under project Contract No. TEC2004-04249-C02-02. The authors would like to express their gratitude to Professor Laszlo Solymar, Professor Ekaterina Shamonina, and the people who participated in the 1st International Workshop on MI Waves (16–19 November 2005, Osnabruek, Germany) whose helpful discussions partially motivated this work. Thanks are also due to their laboratory assistant, Esperanza Rubio, for her help in the fabrication of the lens used in the experiments.

[1] V. G. Veselago, Sov. Phys. Usp. **47**, 509 (1968).
[2] J. B. Pendry, Phys. Rev. Lett. **85**, 3966 (2000).
[3] N. Garcia and M. Nieto-Vesperinas, Phys. Rev. Lett. **88**, 207403 (2002).
[4] D. R. Smith, D. Schurig, M. Rosenbluth, and S. Schultz, Appl. Phys. Lett. **82**, 1506 (2003).
[5] R. Merlin, Appl. Phys. Lett. **84**, 1290 (2004).
[6] R. Marques and J. Baena, Microwave Opt. Technol. Lett. **41**, 290 (2004).
[7] A. Grbic and G. Eleftheriades, Phys. Rev. Lett. **92**, 117403 (2004).
[8] A. N. Lagarkov and V. N. Kissel, Phys. Rev. Lett. **92**, 077401 (2004).
[9] N. Fang, H. Lee, C. Sun, and X. Zhang, Science **308**, 534 (2005).
[10] M. J. Freire and R. Marques, Appl. Phys. Lett. **86**, 182505 (2005).
[11] Z. Lu, J. A. Murakowski, C. A. Schuetz, S. Shi, G. J. Schneider, and D. W. Prather, Phys. Rev. Lett. **95**, 153901 (2005).
[12] R. Marques, F. Mesa, and F. Medina, Appl. Phys. Lett. **86**, 023505 (2005).
[13] S. Maslovski, S. Tretyakov, and P. Alitalo, J. Appl. Phys. **96**, 1293 (2004).
[14] E. Shamonina, V. A. Kailinin, K. H. Ringhofer, and L. Solymar, J. Appl. Phys. **92**, 6252 (2002).
[15] S. A. Ramakrishna, J. B. Pendry, D. R. Smith, D. Schurig, and S. Schultz, J. Mod. Opt. **49**, 1747 (2002).
[16] V. A. Podolskiy and N. A. Kuhta, Appl. Phys. Lett. **87**, 231113 (2005).
[17] V. G. Veselago, Appl. Phys. B: Lasers Opt. **81**, 403 (2005).
[18] F. Mesa, M. J. Freire, R. Marques, and J. D. Baena, Phys. Rev. B **72**, 235117 (2005).
[19] M. C. K. Wiltshire, E. Shamonina, I. R. Young, and L. Solymar, J. Appl. Phys. **95**, 4488 (2004).
[20] W. H. Press, S. A. Teukolsky, W. T. Vetterling, and B. P. Flannery, *Numerical Recipes in FORTRAN*, 2nd ed. (Cambridge University Press, New York, 1994).
[21] It should be mentioned that above this value of k_x the transfer function begins to oscillate. These oscillations can be interpreted as being due to the excitation of MISW for some values of k_x (due to their particular characteristics, the model produces a MISW dispersion relation which is only approximately periodic for high values of k_x). However, as will be explained below, these FHs will not be reproduced by the lens.